Int. J. Thin. Fil. Sci. Tec. **14**, No. 1, 49-55 (2025)

International Journal of Thin Films Science and Technology

http://dx.doi.org/10.18576/ijtfst/140108

First Principal Investigations of Optical Properties of $SrTiO_3$ Doped with C Under bi-axial (001) Strain Regime Influence

Raied A. S. AL-Hamadany

Department of Physics, College of Education for Pure Science, University of Thi-Qar, Thi-Qar, 64001, Iraq

Received: 1 Oct. 2024, Revised: 3 Nov 2024, Accepted: 4 Dec. 2024

Abstract: In this paper, the role of structural distortion originates from strain and its influence on the optical properties of C_{Ti} doped $SrTiO_3$ (STO) was investigated utilizing density functional theory calculations. Real and imaginary parts of dielectric constant as well as refractive index have been examined under range of *c/a* distortion. It has been demonstrated that optical properties of C_{Ti} doped STO in various orientations are substantially impacted within the sign and degree of range of bi-axial strain typical of common substrate materials. Despite the invariable values of in-plane components of static dielectric constant with strain, compressive strain substantially lowered the out-plane component, down to 4.88 for 4%. On the other hand, both components dropped with increasing of tensile strain to be 4.82 and 5.10 for in and out-plane components, respectively. An absorption peak at about 2.5eV appears as the bi-axial compressive strain grows within the (001) plane. A drop in absorption peak at 3 eV for both inter and intra-plane components were obtained when tensile strain increases. The outcomes of this study are anticipated to highlight novel opportunities for the advancement of optoelectronic devices.

Keywords: $SrTiO_3$, strain, oxygen vacancy, carbon, optical properties.

1 Introduction

The Elevated dielectric constant, non-leaner dielectric feature and broad band gap make strontium titanate $SrTiO_3$ as a promising dielectric substance for wide range of electronic applications. These are including resistive switching [1], [2], [3] dynamic random-access memory[4], [5], and gate dielectric. At room temperature, the non-strained $SrTiO_3$ is crystalline in cubic structure having anti-ferroelectric phase. However, the ferroelectric phase will appear under relatively low value of strain[6]. The growth of $SrTiO_3$ thin film in contact with other substances, for instance; metal electrodes, perovskites and semiconductor materials, having lattice parameters differ from $SrTiO_3$. The lattice mismatch imposes thin film of $SrTiO_3$ to be grown under various values and sign of bi-axial strain.

Growth techniques such as chemical vapor deposition[7], pulsed laser deposition[8] and molecular beam epitaxy[9] have a substantial impact on the stoichiometry and purity of $SrTiO_3$. Notably, a number of these methods utilized organic precursors as Sr sources, which, as documented in the literature[10], results in undesirable C-contaminated $SrTiO_3$. Thermodynamic investigation reveals that C might substitute for Ti or O depending upon growth conditions[11]. According to previous investigation, carbon has substantial influence upon electronic and optical properties of zero strain $SrTiO_3$[12] and other perovskite oxides[13], [14], [15].

In complicated oxide thin films, epitaxial strain technique has emerged as an efficient strategy for revealing emerging functional characteristics including multiferroicity, ferromagnetism, or ferroelectricity. Intensive practical and computational investigations have been carried out to understand the impact of strain upon migration of unavoidable defects[16], [17]. Recent theoretical calculations show that the binding of C and native oxygen vacancy is effectively tailored via applying bi-axial strain[18].

The optical absorption of zero strain and pristine-$SrTiO_3$ is limited to an ultraviolet spectrum due to its wide band gap. Experimental measurements on temperature dependence optical properties of $SrTiO_3$ reveal an optical absorption edge near-infrared absorption at temperatures ranging from 4 to 1703 K. The study also concludes that the absorption edge diminishes from 3.25 eV at 4 K to 1.8 eV at 1703 K[19]. An enhancement of phase purity and crystallinity, the $SrTiO_3$ doped Eu annealed at 1000 °C demonstrated by maximum photo-luminescence[20]. The photoconductivity of pure $SrTiO_3$ is affected by the anti-ferro distortive cubic to tetragonal phase transition, which alters the absorption band edge structure in the phase transition region[21]. Despite the large body of investigation regarding optical properties of pristine and doped of $SrTiO_3$, the impact of strain in the presence of C on the optical characteristics $SrTiO_3$ has not been investigated yet.

Optical activity of $SrTiO_3$ is believed to be significantly influenced by combination of unavoidable C defect and

---

*Corresponding author E-mail: raidabass.eps@utq.edu.iq

epitaxial strain. In this paper, the interplay between carbon defect and bi-axial strain and the impact it has upon optical properties of $SrTiO_3$ has been examined. Determining whether bi-axial compressive and tensile strain influences the optical properties of C doped $SrTiO_3$ is primary objective of this study. The results of real and imaginary parts of dielectric constant as well as refractive index of C doped $SrTiO_3$ under range of strain are presented in this paper.

2 Computational Methodology

As implemented in *Ab-Initio* modeling program[22], density functional theory with spin polarized local density approximation[23] was adopted to study the impact of strain on the optical features of C doped $SrTiO_3$. A norm-conserving Pseudopotential was employed to simulate electron-ion interactions[24]. The valence state for each element has been described utilizing for Sr, Ti, and O were $4s^2\,4p^6\,5s^2$ for Sr, $3s^2\,3p^6\,3d^2\,4s^2$ fot Ti, $2s^2\,2p^4$ for O and $2s^2\,2p^2$ for C. Titanium, and oxygen were described using four sets of *s*-, *p*-, and *d*-Gaussian functions, resulting in a total of 40 functions per atom. These functions were employed to represent electronic wave functions using atom-centered Gaussian basis functions[25] . Using the Kohn-Sham potential and a plane-wave expansion of density, the Hamiltonian matrix elements were utilized with a cutoff energy set at 300 Ha. All atoms in the structure were permitted to relax until the optimization criteria of energy and forces were satisfied. The system is considered to be optimized in case the force on each atom is below 10^{-3} a.u. and the difference in energy between sequent iterations is less than 10^{-5} Ha.

The lattice parameter of non-strained $SrTiO_3$ obtained utilizing the computational scheme adopted in this paper was 3.87A which is accords well with previous computational[26] and practical[27] studies. Furthermore, the twisting of neighboring oxygen sub-lattices along [001] direction at small value of strain was described well using the adopted computational approach. The calculated angle of twisting was 1.98° which agrees well with other theory[28]. The bi-axially strained system of non-defective $SrTiO_3$ was modeled by employing super-cell comprising eight formula units of $SrTiO_3$ and lattice vectors 2a[100], 2a[010] and 2a[001]. Two lattice vectors were fixed to each value of strain included in this study. These are (±1%, ±2%, ±3% and ±4%) of lattice constant of zero strained cubic $SrTiO_3$. In each case the energy has been minimized by tuning the third lattice vector. As a result, the strained system is crystalline in tetragonal structure. The strained systems containing C defect were simulated utilizing 160-atoms super cell. The super cell has been generated by repeating the non-primitive 20-atoms in three lattice vectors. The stability of compounds was proven by optimizing all atoms in strained defective systems until the optimization criteria were satisfied. The adopted computational scheme was successfully utilized to investigate mobility of V_o in $SrTiO_3$ under strain regime[16], [17].

The optical properties of medium are theoretically described by adopting the complex dielectric function ε(ω) for different photon frequencies (energies). The function can be written as[29], [30], [31]:

$$\varepsilon(\omega) = \varepsilon_r(\omega) + i\varepsilon_{im}(\omega) \qquad (1)$$

where; $\varepsilon_r(\omega)$ and $\varepsilon_{im}(\omega)$ represent real and imaginary part of dielectric function, respectively. The polarization degree as well as dispersion of photon can be accounted from the real part component ε_r, on the other hand, absorption of photon by the medium can be elucidated from imaginary part component ε_{im} . [32]

$$\varepsilon_{im}\,(\omega)_{\alpha\beta} = \frac{4e^2\pi^2}{\omega^2 m^2}\sum_{i,f}\int \langle f|\,p_\alpha\,|i\rangle\,\langle i|\,p_\beta\,|f\rangle\, W_i\big(1 - W_f\big)\partial\big(E_f - E_i - \hbar\omega\big)d^3k \qquad (2)$$

Where dipole matrix elements are represented by $\langle i|\,p_\beta\,|f\rangle$ and $\langle f|\,p_\alpha\,|i\rangle$ where *i* and *f* are initial and final state between which transition occurs, the Fermi distribution at energy E_i and E_f are W_i and W_f. The variation of imaginary part $\varepsilon_{im}(\omega)$ with frequency can be accounted to calculate the depepence of real part of dielectric function with frequency with assistant of Kramers-Kronig equation [31]:

$$\varepsilon_r(\omega) = 1 + \frac{2}{\pi}\int_0^\infty \frac{\omega'\,\varepsilon_{im}(\omega)\,d\omega}{\omega'^2 - \omega^2} \qquad (3)$$

Other optical properties such as refractive index *n(ω)* can be determined from the complex dielectric function. The refractive index *n(ω)* can also be obtained by adopting equation 4 as[33]:

$$n(\omega) = \big(1/\sqrt{2}\big)\left(\frac{\sqrt{\varepsilon_r^2(\omega) + \varepsilon_{im}^2(\omega)} - \varepsilon_r(\omega)}{2}\right)^{1/2} \qquad (4)$$

3 Results and Discussions

3.1 Assessment of dielectric constant.

As a benchmark for computational scheme adopted in this paper, optical properties of pure, zero-strain STO were calculated. The static dielectric constant $\varepsilon_r(0)$ obtained for pure STO was 5.7. The obtained result in excellent agreement with 5.8 and 5.3 from both theory[34] and experiment[35], respectively. In case of C doped zero-strain STO the calculated value of $\varepsilon_r(0)$ was 5.4. Table.1 shows the in-plane and out-plane of real part of dielectric constant for STO for various lattice distortion represented by *c/a* ratio. As can be seen from the Table.1, distortive STO structure exhibits an anisotropy in the static dielectric constant between in-plane and out-plane values. The anisotropy in the dielectric constant is an outcome of structural distortion which in turn yields displacement of oxygen anion sub-lattices with respect to the direction of bi-axial strain to minimize the energy of distortive system under each value of *c/a*. Clear decreasing in the real part of static dielectric constant with increasing *c/a* ratio of distortion over wide range of lattice distortion. The decreasing can be attributed to the displacement of anion sub-lattices which in turn yields a polarized system within [001] direction in addition to dipole created by substituting of C with Ti.

Table 1: The electronic part of real part of static dielectric constant $\varepsilon_r(0)$ of distorted (due to compressive strain) free defect STO and C_{Ti} doped STO

c/a ratio of distortion	Strain %	ε_r of free defect distorted STO		ε_r of C_{Ti} doped distorted STO	
		In-plane	Out-plane	In-plane	Out-plane
1.019	1%	5.54	5.30	5.35	5.17
1.036	2%	5.50	5.14	5.30	5.00
1.061	3%	5.49	5.02	5.33	4.93
1.092	4%	4.90	5.24	5.32	4.88

The corresponding values of static dielectric constant of distortive free defect and C_{Ti} doped of STO are shown in Table.2 for tensile strained STO structures. *i.e.* for c/a ratio less than 1. As it is shown in table.2 the electronic part of real dielectric constant was different for in-plane and out-plane of strain under tensile bi-axial (001) strain. Furthermore, the values of $\varepsilon_r(0)$ in both directions were generally decreased with increasing values of strain. In comparison with out-plane values of $\varepsilon_r(0)$, the in-plane values decreased more sharply with strain. The divergence in the trend of decreasing of ε between inter and intra plane of strain can be attributed to the mechanisms of polarization originating from interplay between C_{Ti} dopant and strain. As previously reported in the literature, bi-axial tensile strain in STO within (001) plane of strain induced anion sub-lattices to displaced within (001) plane to minimize the energy due to strain. This implies the tensile strain imposed $SrTiO_3$ to be polarized within [100] and [010] directions[16].

Table 2: The electronic part of real part of static dielectric constant $\varepsilon_r(0)$ of distorted (due to tensile strain) free defect STO and C_{Ti} doped STO

c/a ratio of distortion	Strain %	$\varepsilon_r(0)$ of free distorted STO		$\varepsilon_r(0)$ of C_{Ti} doped distorted STO	
		In-plane	Out-plane	In-plane	Out-plane
0.984	1%	5.34	5.52	5.19	5.33
0.970	2%	5.18	5.45	5.06	5.28
0.953	3%	5.02	5.35	4.92	5.20
0.939	4%	4.81	5.24	4.82	5.10

3.2. Imaginary part of dielectric constant

Fig. 1 shows the imaginary part of dielectric function for C doped STO in case of compressive strain within (001) plane of strain. As can be seen from the figure, the behavior of imaginary part of dielectric function has various trends with respect to direction of strain. This implies that the in-plane component of ε_{im} (a) varies in different behavior in comparison with out-plane component (b). It is clear that the in-plane component has two peaks of absorption at an energy range 2 and 4 eV. These two peaks were dramatically affected by increasing strain. Increasing bi-axial compressive strain within (001) planes leads to appearance of absorption peak at around 2.5 eV, while the peak below 4 eV was nearly disappeared with higher value of compressive strain. Furthermore, increasing strain yields a general and small shift for other peaks toward higher energy after 4 eV. The out-pane component of ε_{im} is shown in Fig.1(b). It is obvious that increasing bi-axial compressive strain will suppress the absorption in this direction. In specific, an absorption peak at around 3.5 eV was removed by increasing strain up to 4%. Additionally, there is clear shift of other absorption peaks growing of strain. An enhancement in absorption peaks at around 6.3 and 11.2 eV were approved with strain.

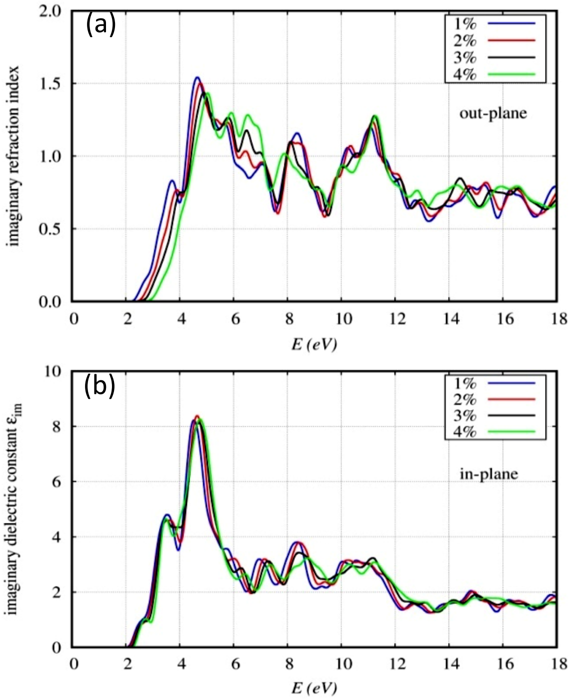

Fig. 1: The imaginary part of dielectric function of C doped compressive strained STO for (a) out-plane of strain and (b) in-plane of strain.

In case of bi-axial (001) tensile strained C doped STO, the imaginary part ε_{im} is plotted in Fig.2(a,b). As the case for bi-axial compressive stain, tensile strain yields an anisotropy in imaginary part of dielectric function in the presence of C_{Ti} in strained STO. The graphs (a) and (b) show multi-noticeable peaks were visible in the plot at different values of energy. These peaks represent the transition from the valence to the conduction band. In general, the interplay between C doping in Ti site and bi-axial strain produces shift of absorption spectrum in both in-plane and out-plane away from visible region. Fig.2(a) shows diminishing in the absorption peak at 3 eV with increasing tensile strain. The corresponding peak in the out-plane component of ε_{im} was also depressed with strain as shown in Fig.2(b). On the other hand, an increase in the intensity of strong peaks at 4.3 eV was obtained with increasing strain for both components and being more for out-plane components. The peaks at around 6 eV show a divergent trend between in-plane and out-plane graph. It was enhanced for in-plane components and diminished for out-plane cases. The opposing trend of ε_{im} in some absorption peaks my attributed to mechanism of polarization originated from the presence of C_{Ti} and its interplay with polarization originates from strain.

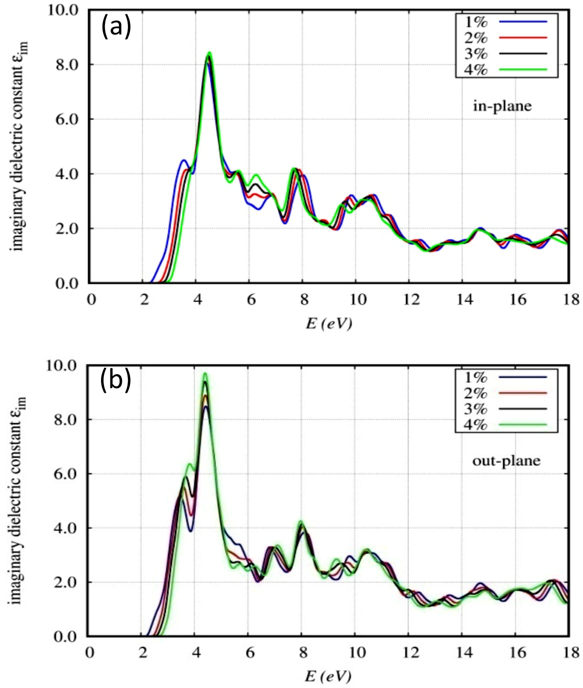

Fig. 2: The imaginary part of dielectric function of C doped tensile strained STO for (a) in-plane of strain and (b) out-plane of strain.

3.3. Refractive index

In advance to impact of C doping and bi-axial strain, the refractive index of pure unstrained STO was calculated to be 2.4. The obtained result was in accordance with previously reported value of 2.37[34], [35]. The real part of complex refractive index of C_{Ti} doped compressive strained STO as function of energies and for values of compressive strain covered in this study is shown in Fig.3(a,b). In case of in-plane component, it was found that static refractive index is invariable with applied compressive strain. By contrast, as shown in Fig.3(b) the corresponding out-plane component was found to decreased with increasing compressive strain from 2.28 for 1% down to 2.18 for 4%. In case of C_{Ti} doped STO under tensile strain, the refractive index the real part of dielectric constant for in-plane and out-plane were plotted in Fig.4(a,b) for C_{TI} doped STO. As shown in Fig.4(a) the static refractive index (at zero energy), were dropped with increasing tensile strain.

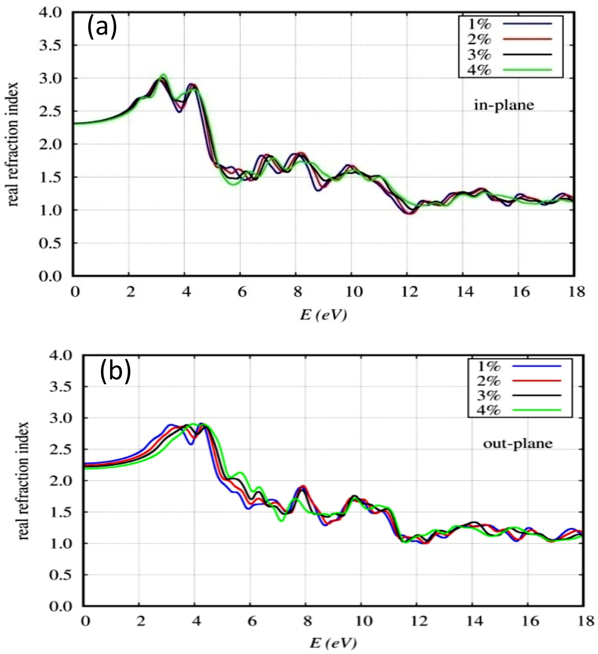

Fig. 3: The real part of refractive index of C doped compressive strained STO for (a) in-plane of strain and (b) out-plane of strain.

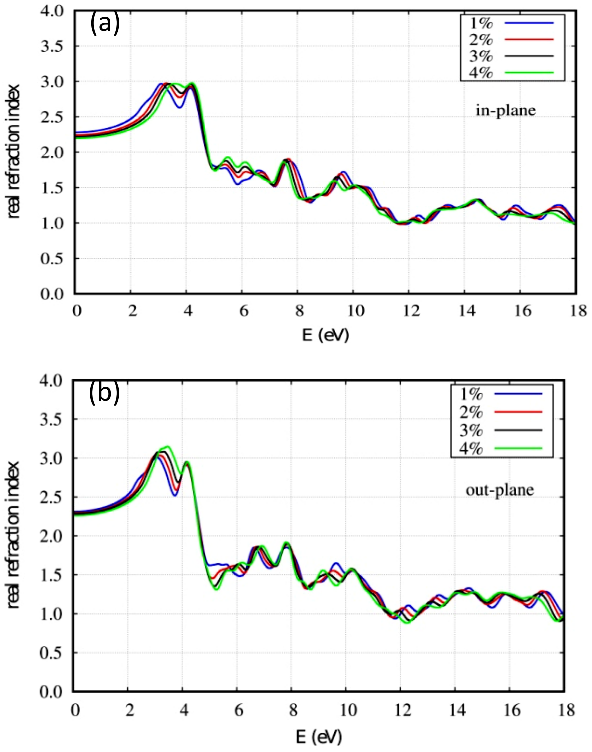

Fig. 4: The real part of refractive index of C_{Ti} doped tensile strained STO for (a) in-plane of strain and (b) out-plane of strain.

Significant outcomes regarding the attenuation of electromagnetic waves traveling through a solid are known to be obtained from the imaginary part of refractive index. The in-plane and out-plane components as a function of photon energy for C_{Ti} doped STO under compressive bi-axal (001) strain were plotted in Fig.5(a,b). It is obvious that the interplay of C_{Ti} and (001) compressive strain produces a shift in the attenuation toward ultraviolet region for both inter and intra-plane of strain. The shifting is more obvious in the out-plane component. Furthermore, Fig.5(a) demonstrates clear increase of attenuation in prominent peak at energy around 4.4 eV for in-plane orientation. Divergent trend of attenuation for corresponding peak in out-plane orientation, in which the attenuation was found to decrease with strain as shown in Fig.5(b). Apart from this peak, strain was found to decrease attenuation for the remaining peaks in in-plane orientation. By contrast, growth of attenuation was observed for remnant out-plane peaks.

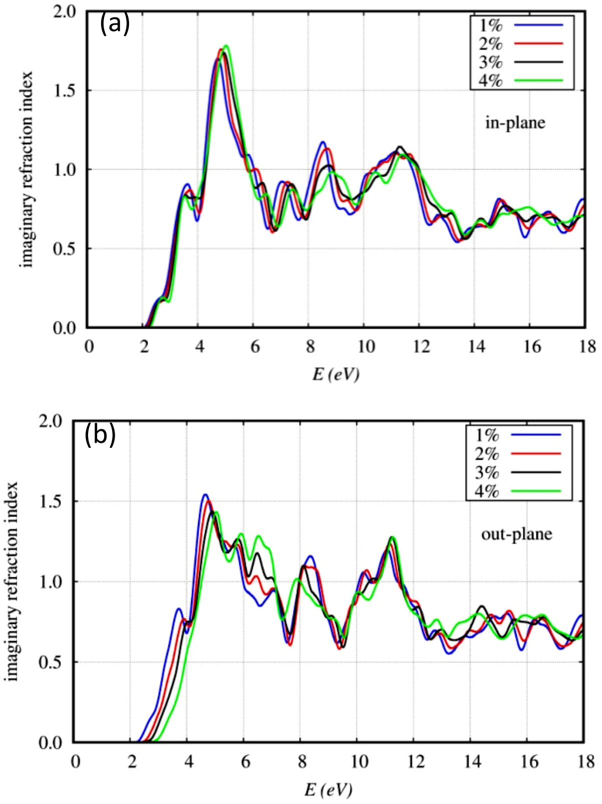

Fig. 5: The imaginary part of refractive index of C doped compressive strained STO for (a) in-plane of strain and (b) out-plane of strain.

The variation of imaginary refractive index with photon energies under tensile strain influence in both orientations were plotted in Fig.6(a,b). The intra-plane component in Fig.6(a) demonstrates suppression of attenuation peak in the visible region with increasing tensile strain. Furthermore, the dominant peak of 4.6 eV was less sensitive to the growth of strain. Strain was found to effectively enhance the attenuation for peak at around 6.3 eV in addition to shifting of peak at 8 eV toward lower photon energy. The inter-plane component of imaginary refractive index shows significant suppression of first peak within visible region and clear enhancement in the intensity of prominent peak at 4.6 eV.

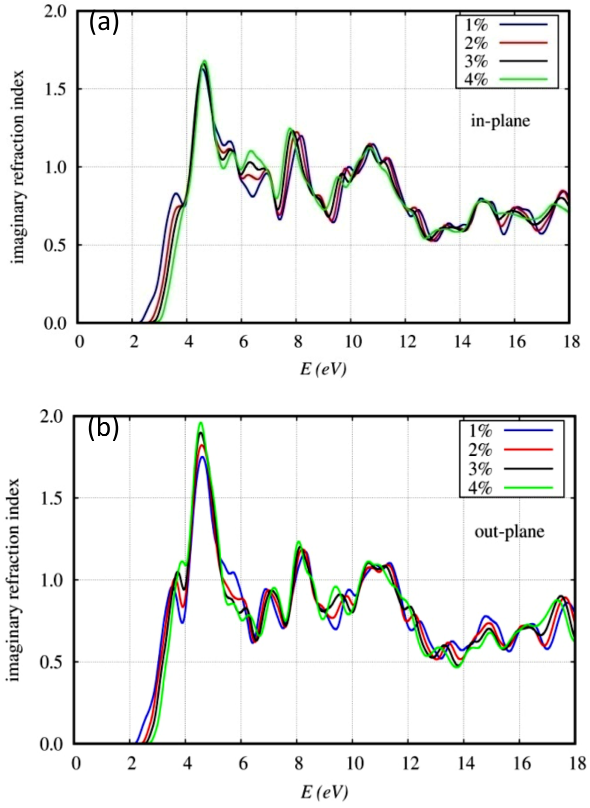

Fig. 6: The imaginary part of refractive index of C doped tensile strained STO for (a) in-plane of strain and (b) out-plane of strain.

In comparison with the influence of bi-axial compressive strain influence, the impact of tensile strain on the behavior of inter-plane components was divergent. The distinction in the impact of different signs of strain on the trend of refractive index is greatly affected by mechanism and direction of polarization of C_{Ti} doped STO system.

4 Conclusions

The impact of bi-axial compressive and tensile strain on the optical properties of C_{Ti} doped STO were investigated utilizing density functional theory calculation. An obvious anisotropy in the behavior between inter and intra plane components of dielectric constant were obtained under all range of strain included in this study. Apart from in-plane $\varepsilon_r(0)$ under compressive strain, all other values of $\varepsilon_r(0)$ were found to decrease with increasing strain in both orientations. Furthermore, divergent influence of strain upon real and imaginary refractive index was obtained. It is interesting to propose that doping of carbon in STO and the application of compressive and tensile bi-axial strain from matching substrate may be employed in conjunction to considerably tune the optical features of STO for various applications. The tuning of optical properties of STO through strain and carbon doping can be adopted as route to better device application such as solar cell and photocatalytic.

References

[1] K. Szot, W. Speier, G. Bihlmayer, and R. Waser, “Switching the electrical resistance of individual dislocations in single-crystalline $SrTiO_3$” *Nat Mater*, **5**, 312-320 (2006).

[2] S. A. Mojarad *et al.*, “Leakage current asymmetry and resistive switching behavior of $SrTiO_3$” *Appl. Phys. Lett.* **101**, 173507 (2012)

[3] M. Janousch, G. I. Meijer, U. Staub, B. Delley, S. E. Karg, and B. P. Andreasson, “Role of oxygen vacancies in Cr-doped $SrTiO_3$ for resistance-change memory,” *Advanced Materials*, **19**, 2232–2235 (2007).

[4] R. Thomas and D. C. Dube, “Electrical properties of $SrTiO_3$ based MIS structures for DRAM applications,” *Ferroelectrics*, **225**, 99-106 (1999).

[5] O. Okhay, A. Wu, and P. M. Vilarinho, “The Mg influence on the properties of $SrTiO_3$ thin films,” *J. Eur. Ceram Soc*, **25**, 3079–3083 (2005).

[6] F. W. Lytle, “X-Ray Diffractometry of Low-Temperature Phase Transformations in Strontium Titanate,” *J Appl Phys*, **35**, 2212–2215 (1964).

[7] Z. Song, B. R. Rogers, and N. D. Theodore, “Spectroscopic ellipsometry characterization of ZrO_2 films on Si(100) deposited by high-vacuum-metalorganic chemical vapor deposition,” *Journal of Vacuum Science & Technology A: Vacuum, Surfaces, and Films*, **22**, 711–718 (2004).

[8] L. Yan *et al.*, “High permittivity $SrHf_{0.5}Ti_{0.5}O_3$ films grown by pulsed laser deposition,” *Appl Phys Lett*, **94**, 23 (2009).

[9] R. A. McKee, F. J. Walker, and M. F. Chisholm, “Crystalline Oxides on Silicon: The First Five Monolayers,” *Phys Rev Lett*, **81**, 3014–3017 (1998).

[10] S. W. Lee *et al.*, “Atomic Layer Deposition of $SrTiO_3$ Thin Films with Highly Enhanced Growth Rate for Ultrahigh Density Capacitors,” *Chemistry of Materials*, **23**, 2227–2236 (2011).

[11] M. Al-Hadidi, J. P. Goss, P. R. Briddon, R. Al-Hamadany, M. Ahmed, and M. J. Rayson, “Carbon impurities in $SrTiO_3$ from first principles,” *Model Simul Mat Sci Eng*, **23**, 1 (2015).

[12] M. Al-Hadidi, J. P. Goss, P. R. Briddon, R. Al-hamadany, M. Ahmed, and M. J. Rayson, “Association of oxygen vacancies with carbon impurity in strontium titanate: first principles calculations,” *Ferroelectrics*, **497**, 9–14 (2016).

[13] M. Al-Hadidi, J. P. Goss, O. A. Al-Ani, P. R. Briddon, and M. J. Rayson, “Density functional calculations of carbon substituting for Zr in barium zirconate,” *J Cryst Growth*, **468**, 728–731 (2017).

[14] M. S. AL-Hadidi, J. P. Goss, P. R. Briddon, R. A. Al-Hamadany, M. E. Ahmed, and M. J. Rayson, “Density functional simulation of carbon at the titanium site in perovskite barium titanate,” *IOP Conf Ser Mater Sci Eng*, **80**, 012002 (2015).

[15] M. Al-hadidi, J. P. Goss, P. R. Briddon, R. Al-hamadany, M. Ahmed, and M. J. Rayson, “First-principles investigation of carbon substitution for lead in ferroelectric lead titanate,” *Ferroelectrics*, **498**, 12–17 (2016).

[16] R. AL-Hamadany, J. P. Goss, P. R. Briddon, S. A. Mojarad, A. G. O’Neill, and M. J. Rayson, “Impact of tensile strain on the oxygen vacancy migration in $SrTiO_3$: Density functional theory calculations” *J Appl Phys*, **113**, 224108 (2013).

[17] R. Al-Hamadany *et al.*, “Oxygen vacancy migration in compressively strained $SrTiO_3$” *J Appl Phys*, **113**, 024108 (2013).

[18] R. A. S. AL-Hamadany, J. P. Goss, and P. R. Briddon, “A route for tunable C-V_o doped perovskite $SrTiO_3$ functionalities through epitaxial strain engineering” *Model. Simul. Mat. Sci. Eng.*, **32**, 065023 (2024).

[19] D. J. Kok, K. Irmscher, M. Naumann, C. Guguschev, Z. Galazka, and R. Uecker, “Temperature-dependent optical absorption of $SrTiO_3$,” *Physica Status Solidi (A) Applications and Materials Science*, **212**, 1880–1887 (2015).

[20] S. Mehra, S. Bishnoi, L. Goswami, G. Gupta, A. K. Srivastava, and S. Narain Sharma, “Detailed chemical mechanism of the phase transition in nano-$SrTiO_3$ perovskite with visible luminescence,” *Inorg Chem Commun*, **120**, 108125 (2020).

[21] F. Rossella, P. Galinetto, G. Samoggia, V. Trepakov, and L. Jastrabik, “Photoconductivity and the structural phase transition in $SrTiO_3$” *Solid State Commun*, **141**, 95–98 (2007).

[22] P. R. Briddon and R. Jones, “LDA Calculations Using a Basis of Gaussian Orbitals,” *physica status solidi (b)*, **217**, 131–171 (2000).

[23] J. P. Perdew and Y. Wang, “Accurate and simple analytic representation of the electron-gas correlation energy,” *Phys Rev B*, **45**, 13244–13249 (1992).

[24] C. Hartwigsen, S. Goedecker, and J. Hutter, “Relativistic separable dual-space Gaussian

pseudopotentials from H to Rn," *Phys Rev B*, **58**, 3641–3662 (1998).

[25] J. P. G. M. J. Shaw and P. R. Briddon, "Marker-Method Calculations for Electrical Levels Using Gaussian-Orbital Basis Sets," Springer, Berlin, Heidelberg, 104, 69–94 (2006).

[26] Y. Yao and H. Fu, "Density-functional theory study of polarization saturation in strained ferroelectrics," *Phys Rev B*, **80**, 035126 (2009).

[27] R. A. Evarestov, S. Piskunov, E. A. Kotomin, and G. Borstel, "Single impurities in insulators: *Ab initio* study of Fe-doped $SrTiO_3$" *Phys Rev B*, **67**, 064101 (2003).

[28] E. Heifets, E. Kotomin, and V. A. Trepakov, "Calculations for anti-ferro distortive phase of $SrTiO_3$ perovskite: hybrid density functional study," *Journal of Physics: Condensed Matter*, **18**, 4845–4851 (2006).

[29] M. A. Ali, N. Khan, F. Ahmad, A. Ali, and M. Ayaz, "First-principles calculations of opto-electronic properties of IIIAs (III = Al, Ga, In) under influence of spin-orbit interaction effects," *Bulletin of Materials Science*, **42**, 36 (2019).

[30] C. Sifi *et al.*, "First principle calculations of structural, electronic, thermodynamic and optical properties of $Pb_{1-x}Ca_xS$, $Pb_{1-x}Ca_xSe$ and $Pb_{1-x}Ca_xTe$ ternary alloys," *Journal of Physics Condensed Matter*, **21**, 19 (2009).

[31] F. Drief, A. Tadjer, D. Mesri, and H. Aourag, "First principles study of structural, electronic, elastic and optical properties of MgS, MgSe and MgTe," in *Catalysis Today*, **89,** 343–355 (2004).

[32] R. Husin, F. W. Badrudin, M. F. M. Taib, and M. Z. A. Yahya, "Effects of strain on electronic and optical properties of $LiNbO_3$: A first principles study," *Mater Res Express*, **6**, 11 (2019).

[33] S. Azam *et al.*, "DFT study of the electronic and optical properties of ternary chalcogenides AlX_2Te_4," *Mater Res Express*, **6**, 116314 (2019).

[34] R. Ahuja, O. Eriksson, and B. Johansson, "Electronic and optical properties of $BaTiO_3$ and $SrTiO_3$," *J Appl Phys*, **90**, 1854–1859 (2001).

[35] M. Cardona, "Optical Properties and Band Structure of $SrTiO_3$ and $BaTiO_3$", Phys. Rev.,**140**, A651 (1965).